

Expanding the reach of diffusing wave spectroscopy and tracer bead microrheology

M. Helfer,¹ C. Zhang,¹ and F. Scheffold¹

¹*Department of Physics, University of Fribourg, Chemin du musée 3, 1700 Fribourg, Switzerland*

(*Frank.Scheffold@unifr.ch)

(Dated: February 24, 2025)

Diffusing Wave Spectroscopy (DWS) is an extension of standard dynamic light scattering (DLS), applied to soft materials that are turbid or opaque. The propagation of light is modeled using light diffusion, characterized by a light diffusion coefficient that depends on the transport mean free path ℓ^* of the medium. DWS is highly sensitive to small particle displacements or other local fluctuations in the scattering properties and can probe subnanometer displacements. Analyzing the motion of beads in a viscoelastic matrix, known as one-bead microrheology, is one of the most common applications of DWS. Despite significant advancements since its invention in 1987, including two-cell and multi-speckle DWS, challenges such as merging single and multi-speckle data and limited accuracy for short correlation times persist. Here, we address these issues by improving the two-cell Echo DWS scheme. We propose a calibration-free method to blend and merge Echo and two-cell DWS data and demonstrate the use of regularized inversion algorithms to enhance data quality at very short times. Building on this, we introduce stable corrections for bead and fluid inertia, significantly improving the quality of microrheology data at high frequencies.

I. INTRODUCTION

Diffusing Wave Spectroscopy (DWS) is a standard light scattering technique used to study the dynamics of colloids, colloid-polymer mixtures, surfactant solutions and other soft matter systems that display interesting complex relaxation dynamics [1–13]. Introduced in 1987 [14, 15] DWS is an extension of the standard dynamic light scattering (DLS) approach [16]. In contrast to DLS it is applied to materials that are turbid or opaque. In such materials, light is not scattered only once, as is the case in DLS, but multiple times. The propagation of light is often modeled using light diffusion characterized by a light diffusion coefficient that depends on the transport mean free path ℓ^* of the medium. Coherent light becomes dephased due to the motion of the scatterers in the medium [17–19], which can be quantified by analyzing the Intensity time auto-Correlation Function (ICF) of scattered light, analogous to the case of DLS.

DWS is commonly applied to samples such as dense suspensions and emulsions [11, 12, 20–24]. Alternatively, it can be applied to transparent samples by adding tracer beads that sense the dynamic environment of the medium [5, 7, 13, 22, 25–29]. The advantage of DWS over DLS is that it can be applied to turbid media that are not accessible to classical DLS due to dominant multiple light scattering [30]. Additionally, DWS is highly sensitive to small particle displacements or other local fluctuations of the scattering properties. DWS can probe subnanometer displacements, as demonstrated by Weitz et. al. in 1989 shortly after the method was introduced [31]. The high sensitivity of DWS is especially useful when tracer beads are embedded in a viscoelastic medium of interest. DWS can measure viscoelastic solids with elastic moduli up to 100 kPa or more [32] and can study relaxations on microsecond timescales, such as Rouse-Zimm and bending modes of polymer dynamics [6, 7, 33].

Analyzing the motion of beads in a viscoelastic matrix is known as (single) bead microrheology [5, 26, 28], which is one of the most common applications of DWS. Pioneering work by Mason, Weitz, and others showed that the mean

squared displacements of the beads $\langle \Delta r^2(t) \rangle$ can be directly converted into the linear viscoelastic spectrum, or complex modulus $G^*(\omega) = G'(\omega) + iG''(\omega)$, of the materials if the bead radius is known [25, 34, 35]. DWS provides access to this information from the sub-microsecond scale to seconds and minutes, opening up opportunities in rheology to study viscoelastic moduli over an enormous range of frequencies with a single measurement [7]. Several reviews of the theory underlying the method, along with numerous examples of its applications, have been published. We refer the reader to the literature for further details [1, 3–5, 13, 27, 28].

Since the invention of DWS in 1987, several substantial improvements to the method have been made. The original approach relied on taking time averages of the intensity correlation function (ICF), which requires the sample to be in a liquid state. Two-cell DWS, introduced in 2000 [36], and other ensemble averaging approaches [37, 38] provided access to short correlation times for solid, nonergodic systems. Multi-speckle DWS, using either a camera or the Echo-scheme, was introduced in the early 2000s and it provides access to longer correlation times for highly viscous or viscoelastic solids such as glasses and gels [39–44]. In 2017, an automated method for determining the optical transport and absorption mean free paths for absorbing and non-absorbing samples was developed [29]. These advancements have made it possible to access the ICF over a range from typically 10 ns to tens of seconds or more while keeping the measurement time on the order of a few minutes. Only when studying even longer relaxation times does the measurement time need to be further increased. Despite these significant advances, shortcomings in the implementation of these methods can still lead to errors or reduced data quality. Moreover, access to very short correlation times is hindered by photon shot noise and the need to normalize the ICF, which, in its current implementation, introduces bias.

In the present work, we address these problems and propose two substantial improvements to the implementation of the two-cell Echo DWS measurement scheme, which is the most common implementation of DWS. We present a calibration-

free method to blend and merge the Echo and two-cell DWS measurements. Additionally, we demonstrate that using an unbiased fit to the intensity correlation function (ICF) at short times using a regularized inversion algorithm such as CONTIN can substantially improve the quality of the data at very short times. Based on this approach, we further demonstrate that a full correction for the bead and fluid inertia can be applied in a stable manner, further enhancing the microrheology data quality at short times.

II. METHOD

Conventional photon correlation spectroscopy (PCS), as used in DLS or DWS, relies on time-averaging the photon correlation function recorded by a single-photon detector and processed using hardware electronic or software correlator [16]. Echo-DWS employs a multi-speckle Echo detection scheme to accurately measure slow relaxation dynamics, typically for times equal to or longer than a tenth of a second. Multi-speckle DWS is achieved by illuminating a (e.g. ground-glass) diffuser with a laser and then spinning or oscillating the glass at the desired frequency $1/\tau_{\text{Echo}}$ [42, 44]. The modulated speckle beam is used to illuminate the sample of interest. The resulting, properly ensemble averaged, echo correlation function is combined with a two-cell DWS measurement [17, 36, 41], where the ground glass is displaced slowly to force the decay of the intensity autocorrelation function (ICF) of the sample on typical time scale τ_{TC} . These approaches ensure proper ensemble averaging, achieved by illuminating the sample with a larger number of different speckle fields. Both measurements are then combined to obtain a single ICF spanning correlation times from typically 12.5 ns to ten seconds or more, covering an impressive nine orders of magnitude in relaxation times. The method, as it is currently used, however suffers from two main limitations, both of which we address here.

A. Blending and Merging the Two-Cell and Echo Signals

The shortest time accessible to Echo-DWS is determined by the periodicity of the diffuser's rotation or oscillation. Since this requires mechanically oscillating or rotating an object weighing a few grams with high precision, the minimum accessible echo time is currently limited to just under a tenth of a second. Realizing somewhat shorter times is possible but the procedure tends to be less stable and more prone to drift, or it requires more complex and expensive equipment to provide the required accuracy. In this study, we use an already elevated frequency of 25 Hz, corresponding to the first echo located at $\tau_{\text{Echo}} = 0.04$ seconds. Commercial instrumentation, such as the DWS RheoLab (LS Instruments, Switzerland), typically operates with echo-correlation times starting at 0.1 or 0.2 seconds.

To be able to merge the Echo-DWS and the two-cell DWS intensity correlation functions, $g_2(t) - 1$, the forced decay of the latter must be set to a time similar to or larger than τ_{Echo} .

For comparison, in the original two-cell DWS study by Romer et al. [36], the value of τ_{TC} was six times greater than the final data point reported for $g_2(t) - 1$. Using the multiplication rule proposed in ref. [17], the relation

$$g_2^{\text{TC}}(t) - 1 = (g_2(t) - 1) \times (g_2^{2\text{nd}}(t) - 1) \quad (1)$$

can be applied to the two-cell data. We note that, for clarity, in this section, we ignore the influence of the experimental coherence factor, β and set it to one. By dividing the measured $g_2^{\text{TC}}(t) - 1$ by $g_2^{2\text{nd}}(t) - 1$, one can recover the true intensity correlation function $g_2(t) - 1$, where $g_2^{2\text{nd}}(t) - 1$ is obtained independently through a long calibration measurement on a solid reference sample, such as a slab made from Teflon or colloidal beads embedded in a solid epoxy matrix.

The maximum time to which the true intensity correlation function can be extracted from TC-DWS reliably depends on the accuracy of the division based on Eq. (1). Unfortunately, the accuracy is often not very high, primarily due to the limited time available for averaging during the recording of $g_2^{\text{TC}}(t) - 1$. In practice, the forced decay of $g_2^{\text{TC}}(t) - 1$ exhibits significant variations, and dividing by the reference sample measurement, $g_2^{2\text{nd}}(t) - 1$, frequently results in visible perturbations of the ICF around τ_{Echo} . Moreover if two datasets are joined at τ_{Echo} without substantial overlap, any deviation of the experimental $g_2(t) - 1$ from the properly ensemble-averaged value leads to a noticeable kink in the final correlation function used for further analysis, see also Fig. S1. If a greater data overlap is to be achieved using the common method, the measurement time will have to be further extended, which is again not practical.

Here, we propose an alternative approach based on dividing the measured correlation function by the echo correlation function. The latter is, up to a prefactor A , proportional to the true correlation function. Furthermore, the echo-ensemble average is generally accurate due to the large number of independent realizations probed during a single echo interval [42]. Thus,

$$\frac{g_2^{\text{TC}}(t) - 1}{g_2^{\text{Echo}}(t) - 1} = A(g_2^{2\text{nd}}(t) - 1) = Ae^{-(t/\tau_{\text{TC}})^2}. \quad (2)$$

Here, the decay due to the second term is modeled as an exponential function, $e^{-(t/\tau_{\text{TC}})^2}$. The $(t/\tau_{\text{TC}})^2$ -term is attributed to the unidirectional motion of the diffuser.

Using this procedure, we obtain an effective second-cell decay characteristic of the measurement we carried out, removing the need for a calibration sample. We extract A and τ_{TC} from a fit to the data over e.g. six data points, and then use τ_{TC} to correct $g_2^{\text{TC}}(t) - 1$ and A to adjust the amplitude of $g_2^{\text{Echo}}(t) - 1$. Finally, we combine the data over the fitting region, and then append the remaining data points from the echo measurement. This approach ensures a smooth crossover between the two measurements without any discontinuities.

B. Analysis of the short-time correlation function decay without bias

One of the key features of DWS is the ability to measure tiny displacements of particles or other local rearrangements. DWS enables measurements of sub-diffusive motion on nanometer length scales using visible light as a probe. In DWS-based microrheology, relaxations on (sub-)microsecond time scales correspond to frequencies in the viscoelastic spectra of 10^6 rad/s and above, which no other laboratory technique can measure. Displacement of particles on these time scales is sub-Brownian which means it is increasingly affected by the finite inertia of the tracer particles or beads and the surrounding fluid, which we will discuss in the next section. First, we focus on the accurate measurement of short-time decay.

DWS probes $[k(L/\ell^*)]^2 \langle \Delta \bar{r}^2(t) \rangle$ over a specific range determined by the measurement precision, where $k = 2\pi n/\lambda$ is the wavenumber of scattered light in the host medium with a refractive index n . By increasing the optical density L/ℓ^* of the sample—either by increasing the cell thickness L or by lowering ℓ^* through an increase in tracer bead concentration—one can shift the window of accessible mean squared displacements to smaller values (and shorter time scales). However, this comes at the expense of reduced sensitivity to larger displacements.

For $t \rightarrow 0$ the ICF tends to a constant value of $g_2(0) - 1 = \beta$ where $\beta \lesssim 1$ denotes the coherence factor of the detection fiber optics. In a typical DWS microrheology experiment, for short relaxation times up to some ten or hundreds of microseconds, the bead motion often leads to relatively minor decays of the measured ICF, often only by a few per cent. Extracting $\langle \Delta \bar{r}^2(t) \rangle$ from these minor decays is strongly affected by the accuracy with which one can determine β and by the significant photon shot noise at short correlation lag times [45]. The normalization to determine β is usually performed by extrapolating the measured $g_2(t)$ to $t = 0$ using a linear or polynomial fitting function. Once β is known, the normalized ICF is used to determine e.g. $\langle \Delta \bar{r}^2(t) \rangle$. This standard procedure suffers from two problems. First, the choice of the polynomial order used for the fit, as well as the time interval used for fitting the data, influences the exact value of β that is obtained, thereby introducing bias. Here, it is important to note that, due to the inertia of the beads and the fluid, the short-time dynamics are rather complex even for simple colloidal suspensions in water, and thus no simple temporal scaling for the actual $\langle \Delta \bar{r}^2(t) \rangle$ can be assumed [20, 31, 46]. Second, since the raw ICF is only divided by β but otherwise used as-is for further analysis, the experimental noise is not removed. As a result, the data fluctuates around the mean and sometimes even reaches values larger than one, which is unphysical and leads to invalid data points for the bead mean squared displacement $\langle \Delta \bar{r}^2(t) \rangle$ and further introduces bias. This, in turn, creates difficulties in extracting the rheological information and performing the inertia corrections discussed in the following section.

To overcome this problem we propose using an essentially unbiased fit to the ICF at short times with a regularized inversion algorithm such as the well known CONTIN algorithm,

which, as we show substantially improves the quality of the data at very short times. The popular open-source CONTIN algorithm by Provencher [47] inverts the following expression for the field correlation function, expressed as a spectrum over exponential decays

$$g_1(t) = \frac{\int f(\Gamma) \exp(-\Gamma t) d\Gamma}{\int f(\Gamma) d\Gamma}, \quad (3)$$

where Γ denotes the decay rate. This approach was developed to model the normalized decay of a DLS field-correlation function $g_1(t)$ of light singly scattered from a polydisperse or multimodal suspension of colloidal particles undergoing Brownian motion. The measured intensity correlation function (ICF) $g_2(t)$ is related to the field correlation function via the Siegert relation: $g_2(t) = 1 + \beta g_1^2(t)$ [16, 47]. Since the inversion for incomplete and noisy data is ill-posed, the algorithm employs certain regularization methods to obtain a stable fit. Numerous works have discussed improvements to the fit accuracy and stability, see Scotti et al. [48] and references therein. In the present context, our aim is not to extract or to analyse the relaxation spectrum $f(\Gamma)$, but rather to use this established method to obtain an unbiased (or at least much less biased) fit to the experimental data. This fit removes experimental noise at short times, allows extrapolation to $t = 0$ to accurately determine β and the normalized ICF can subsequently be used for further processing.

C. One-bead microrheology with inertia corrections

The time relaxation of the intensity correlation function (ICF) is determined by the motion of the beads and the light scattering process. Precise analytical formulas have been developed to extract the bead mean square displacement (MSD) from the measured DWS intensity autocorrelation functions in transmission geometry. The measured mean square displacement, in turn, is determined by the linear viscoelastic properties of the host medium and, at short times, also by the inertia of the bead and the fluid. Particle interactions, convection or flow, and phase separation can also influence the particle motion, but these effects will not be discussed here [3, 13]. Ignoring such effects, the analysis procedure proceeds as follows: First, we extract the mean squared displacement (MSD), $\langle \Delta \bar{r}^2(t) \rangle$, from the ICF. Next, we remove the contributions due to bead and fluid inertia to obtain the unperturbed viscoelastic spectra of the (complex fluid) host medium. The different steps and approximations made will be discussed in the following. Additionally, we will highlight the importance of clean and low-noise data to stably perform this analysis.

1. Mean squared displacement

We first convert the experimental data to the MSD using Eq. (4) taken from ref. [3], assuming that the slab thickness L , the sample's transport mean free path ℓ^* and the wavenumber k are known. Since we study non-absorbing samples, we

neglect the effects of absorption, but these can be easily incor-

porated if required [29].

$$g_2(t) - 1 = \left\{ \frac{\frac{L/\ell^* + 4/3}{z_0/\ell^* + 2/3} \left(\sinh \left[\frac{z_0}{\ell^*} \sqrt{k^2 \langle \Delta \bar{r}^2(t) \rangle} \right] + \frac{2}{3} \sqrt{k^2 \langle \Delta \bar{r}^2(t) \rangle} \cosh \left[\frac{z_0}{\ell^*} \sqrt{k^2 \langle \Delta \bar{r}^2(t) \rangle} \right] \right)}{\left(1 + \frac{4}{9} k^2 \langle \Delta \bar{r}^2(t) \rangle \right) \sinh \left[\frac{L}{\ell^*} \sqrt{k^2 \langle \Delta \bar{r}^2(t) \rangle} \right] + \frac{4}{3} \sqrt{k^2 \langle \Delta \bar{r}^2(t) \rangle} \cosh \left[\frac{L}{\ell^*} \sqrt{k^2 \langle \Delta \bar{r}^2(t) \rangle} \right]} \right\}^2 \quad (4)$$

If internal reflections are absent or neglected, $z_0/\ell^* \simeq 2/3$. In our case, we consider a glass cuvette in air; thus, $z_0/\ell^* \simeq 2$, a value derived from the work of Durian et al. [49]. The larger L/ℓ^* , the less important the choice of z_0 becomes [13]. We note that, for each value of t , we obtained a precise value for $\langle \Delta \bar{r}^2(t) \rangle$, and there is no fitting or ambiguity involved in this process.

2. Microrheology Routine

We use the following microrheology routine, based on the work by Mason [50], to determine the apparent complex modulus (inertia-affected) $Z^*(\omega)$ from the mean squared displacement data $\langle \Delta r^2(t) \rangle$, determined in the previous step, as follows:

$$\alpha(\omega) = \left. \frac{d \ln \langle \Delta \bar{r}^2(t) \rangle}{d \ln t} \right|_{t=1/\omega}, \quad (5)$$

$$i\omega F_u \{ \langle \Delta \bar{r}^2(t) \rangle \} \approx \langle \Delta \bar{r}^2(1/\omega) \rangle \Gamma[1 + \alpha(\omega)] i^{-\alpha(\omega)}, \quad (6)$$

and finally

$$Z^*(\omega) = \frac{k_B T}{\pi a \omega F_u \{ \langle \Delta \bar{r}^2(t) \rangle \}}. \quad (7)$$

where a denotes the radius of the tracer beads. Eq. (7) is also known as the generalized Stokes Einstein equation (GSE) (in the Fourier domain) [28, 50].

3. Inertia correction

At very short times, the common description of thermal Brownian motion breaks down, a phenomenon that has been well-known since Einstein's work in 1905 [51]. The transition from ballistic to Brownian dynamics, which is strongly affected by hydrodynamics, has garnered renewed attention over the past decade [31, 52, 53]. Neglecting these contributions in the microrheology analysis can result in significant errors. Properly accounting for these effects at short times, corresponding to high frequencies (ω) when determining the complex modulus $G^*(\omega)$, enables the extraction of critical data that would otherwise be challenging or impossible to obtain.

The inertia correction formula used in the present study is based on the work of Domínguez-García et al. [54]. The complete theoretical treatment applied here was first developed and published by Schieber et al. [55]. Prior to that, an (iterative) approximative algorithm to correct for inertia effects was developed in Willenbacher et al. [7] and similarly employed by Mizuno et al. [56]. From the apparent complex modulus $Z^*(\omega)$, extracted from the experimental data via Eq. (7), we can calculate the host medium's complex modulus as follows:

$$G^*(\omega) = Z^*(\omega) + \frac{m^* \omega^2}{6\pi a} + \frac{a^2 \omega^2}{2} \left[\sqrt{\rho^2 - \frac{2\rho}{3\pi a^3} \left(\frac{6\pi a}{\omega^2} Z^*(\omega) + m^* \right)} - \rho \right], \quad (8)$$

The effective mass of the tracer beads is:

$$m^* = \frac{4\pi a^3}{3} \rho_b + \frac{2\pi a^3}{3} \rho, \quad (9)$$

where ρ_b is the bead density and ρ is the medium density in kg/m^3 . Both $G^*(\omega)$ and $\langle \Delta \bar{r}^2(\omega) \rangle$ are complex functions, which can be evaluated using computational tools such as Mathematica (Wolfram, USA) [57]. We can then obtain:

- The absolute value $|G^*(\omega)|$,
- The storage modulus $G'(\omega) = \text{Re} G^*(\omega)$,

- The loss modulus $G''(\omega) = \text{Im} G^*(\omega)$.

III. RESULTS - EXPERIMENTAL VALIDATION

A. Sample

We study DWS microrheology on a wormlike micellar sample discussed extensively in previous work [7, 40, 58, 59]. To this end we prepare an aqueous solution of cetylpyridinium chloride and sodium salicylate (100 mM CPyCl–100

mM NaSal) at different temperatures. We mix the sample with polystyrene beads with a diameter of 420 nm to a final concentration of slightly below 1% in volume. We prepare the sample such that the micellar concentration relative to the aqueous solvent phase is kept constant. The sample displays nearly perfect Maxwellian behavior at low frequencies or slow relaxation times and exhibits the characteristic dynamics of polymer relaxations at short times. It is a strongly viscoelastic liquid with a terminal relaxation time that reacts to temperature over a wide range. Here, we use it as a model system to demonstrate our improved implementation of two-cell echo diffusing wave spectroscopy for different terminal relaxation times larger than or comparable to τ^{TC} .

B. Experimental Setup

We carry out DWS experiments in transmission geometry, where an expanded incident laser beam illuminates the sample contained in a rectangular glass cuvette, with a width larger than its thickness L . The diffusely scattered light is recorded on the opposite side, in transmission, using a single-mode optical fiber. We use a classical custom-made DWS setup with a Helium-Neon gas laser operating at a 632.8 nm wavelength emission. The collimated laser beam is directed towards a 12.5mm diameter holographic diffusor (Edmund Optics, UK) with a 5° diffusing angle. Compared to ground or opal glass diffusers, holographic diffusers offer higher light transmission and a more even distribution of light. They provide control over the diffusion angle, eliminating the need for an additional collimation lens between the diffusor and the sample. In our setup the diffusor is mounted on a Voice Coil Actuated Flexure Scanner (VCFL35, Thorlabs, USA). The scanner is operated at 25 Hz using a function generator. The light diffracted from the diffusor in the forward direction forms a random speckle field that we use to illuminate the sample cuvette. The sample is contained in 12.5 mm wide, 10 mm inner width glass cuvette (Hellma, Germany) with a path length of $L = 2$ mm. For the chosen distance of the ground glass from the cuvette, the speckle beam size is comparable in width to the cuvette. We place a black circular aperture with an 8 mm opening in front of the cuvette to avoid illuminating the cuvette edges.

The light transmitted through the multiple scattering sample is detected in the far field on the other side using a single-mode fiber (OZ Optics, Canada). The single-mode fiber is split 50/50, and each arm is connected to an APD single-photon detector (Excelitas, USA). Using a digital correlator (LS Instruments, Switzerland), we calculate the pseudo cross-correlation function of the scattered photons, which is equal to the photon autocorrelation function but eliminates detector noise (also known as afterpulsing effects). The setup is similar to the one shown in Figure 1 of reference [42].

We operate the voice coil scanner in two modes. In slow mode, the ground glass motion leads to a slow decay of the intensity correlation function (ICF) on a timescale of τ^{TC} but does not affect the short-time dynamics except for providing proper ensemble averaging of the correlation function,

Fig. 1 (a). We perform an approximate normalization of $g_2^{\text{TC}}(t) - 1$ by dividing the data by the values recorded around $t = 10^{-7}$ s, which typically range between 0.9 and 0.95. In fast mode, the periodic oscillation of the ground glass with a period of $\tau^{\text{echo}} = 0.04$ sec leads to correlation echoes [42–44], Fig. 1 b), which we detect using a linear correlator scheme configured in the digital correlator. This scheme provides a time resolution of 1 μ s and spans 16 channels centered around $\tau^{\text{echo}} = 0.04$ sec and multiples thereof. From a Lorentzian fit of the detected correlation echoes, we determined the total area of the echo peak. This total area is a robust measure of the intensity correlation function, modulo an unknown prefactor $1/A$ [42, 43].

C. Merging two-cell DWS and Echo data

We first generate an interpolating function for $g_2^{\text{TC}}(t) - 1$ in Mathematica based on the data recorded using a multiple-tau layout of correlation lag times [60]. Mathematica employs piecewise polynomial interpolation (cubic interpolation for smoothness) to construct the interpolating function [57]. This function is then used to calculate the values of $g_2^{\text{TC}}(t) - 1$ at $t = \tau^{\text{echo}}$ and its multiples in the linear lag time scheme of the echo correlation function. To merge the two datasets, we use the first six echo data points from $t = \tau^{\text{echo}} = 0.04$ s to $t = 6\tau^{\text{echo}} = 0.24$ s. The choice of six is ad hoc, but it is evident that at least a few overlapping data points are necessary to blend the two measurements effectively, while selecting an excessively large number of overlapping points provides little benefit. For these six points $i = 1, 2, \dots, 6$ we calculate the ratio $[g_2^{\text{TC}}(i \times \tau^{\text{Echo}}) - 1] / [g_2^{\text{Echo}}(i \times \tau^{\text{Echo}}) - 1]$. As shown in the inset of Fig. 1 (b), we find that for our (conservative) choice of $\tau^{\text{TC}} \simeq 0.7$ s, this range of data points is well described by Eq. (2), and we extract the parameters A and τ_{TC} from a fit to the data. Finally, we multiply the full dataset for $g_2^{\text{Echo}}(t) - 1$ by A , divide the dataset $g_2^{\text{TC}}(t) - 1$ by $e^{-(t/\tau_{\text{TC}})^2}$, and truncate it at $t = 6\tau^{\text{echo}} = 0.24$ s. We merge both datasets into one, and the excellent result is shown in Figure 1(c). For comparison with the conventional approach see also Fig. S1.

We also tested a more aggressive setting $\tau^{\text{TC}} \simeq 0.28$ s and find equally good agreement as shown in the Supplemental Material, Table S1 and Figures S2 and S3. Our results suggest that as long as $\tau_{\text{TC}} \geq 6\tau^{\text{Echo}}$, corresponding to a second-cell ICF decay of no more than $1/e$ for the last overlapping data point, the parameters A and τ_{TC} can be extracted accurately, and the data can be blended and merged smoothly. The statistical noise concerning A and τ_{TC} is now reduced from 10% to about 5%, see Table S1. Access to such smaller τ_{TC} values implies that a shorter measurement duration can be sufficient to obtain data of comparable quality to that shown in Figure 1. This enhances the suitability of DWS microrheology for monitoring time-evolving processes, such as gelation, a long-standing objective in soft matter research [61, 62]. Previously, limitations in data precision hindered the effectiveness of this approach. The present implementation overcomes these constraints, and while further testing and parameter op-

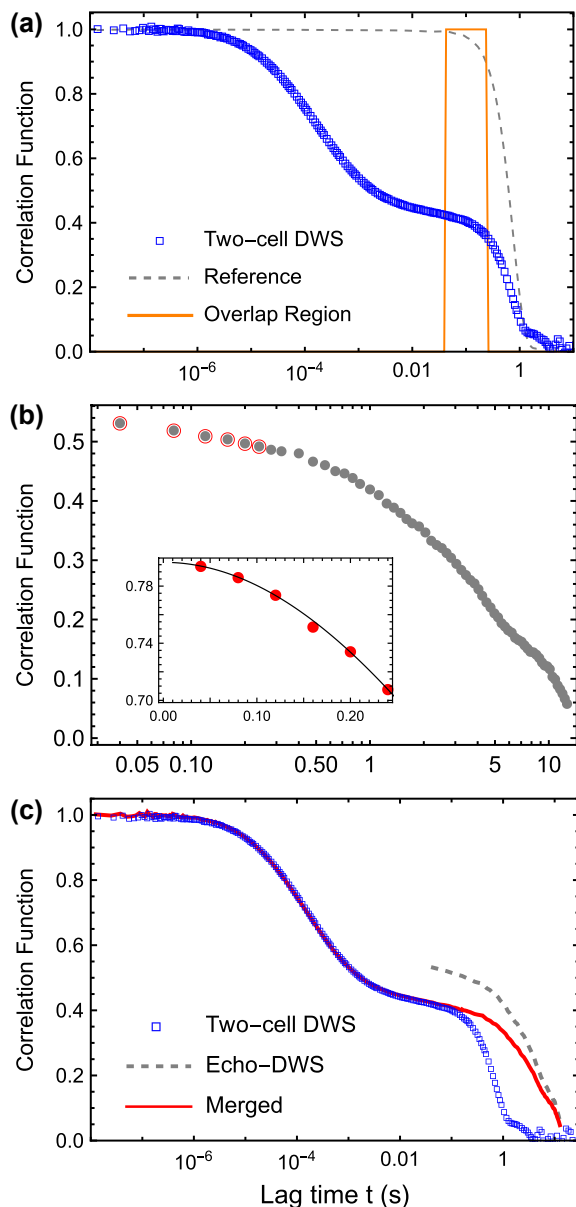


FIG. 1. (a) Two-cell correlation function $g_2^{\text{TC}}(t) - 1$ recorded over 300 seconds for a wormlike micellar solution at $T = 20^\circ\text{C}$ with polystyrene tracer beads embedded. The overlap region is marked with an orange line. The dashed line shows the correlation function measured for a solid piece of Teflon, recorded over 3 hours and following Eq. (2) with $A = 1$ and $\tau_{\text{TC}} = 0.708$ s. (b) Echo two-cell DWS for the same sample recorded over 60 seconds, with data up to 12 seconds. The oscillation period is $\tau_{\text{Echo}} = 0.04$ s. Inset: Ratio of the two-cell correlation function to the echo correlation function. Line: Best fit to the data with $A = 0.797$ and $\tau_{\text{TC}} = 0.697$ s using Eq. (2). From nine datasets taken at temperatures 20° , 25° and 30°C we find $\langle A \rangle = 0.8468 \pm 0.0774$, $\langle \tau_{\text{TC}} \rangle = 0.681 \pm 0.0673$ or a statistical variation of about 10% for both parameters. (c) Blending and merging two-cell DWS and echo data. Blue open square: Two-cell correlation function. Dashed line: Echo correlation function. Red line: Merged correlation function obtained by multiplying the echo data by the parameter A and dividing the two-cell data by the exponential function, Eq. (2) (up to $t = 6 \times \tau_{\text{Echo}}$) then merging the two data sets.

timization are beyond the scope of this work, it is conceivable that a time resolution on the order of a minute or two could be achieved, enabling high-quality and stable broadband DWS microrheology data acquisition during relatively fast gelation processes.

D. DWS microrheology and inertia correction

1. Data preparation

In the previous section, we demonstrated how to blend and merge the two-cell and echo measurements without the need for a calibration sample, achieving a smooth and steady transition between the two datasets. We note that the first few echo data points are relatively widely spaced on the time axis, but they are now combined with the two-cell data over the same time range and instead form a fairly dense dataset. Echo data at larger times are densely spaced compared to the multiple-tau channel layout. This outcome is important, as the particle mean square displacement (MSD) we study is typically represented in a logarithmic format, and microrheology routines often rely on analyzing derivatives of the logarithm of the mean squared displacement, Eq. 5. An unevenly spaced distribution of time channels around τ_{Echo} can introduce errors and inconsistencies in the data processing.

2. CONTIN fitting

We use this dataset as input for a fit with CONTIN. If the processing is restricted to short times, smaller than $t = 5 \times 10^{-4}$ s, we consistently obtain an excellent fit to the data. However, if we attempt to fit the entire dataset with CONTIN, the fit does not always converge, and visible deviations between the fit and the data occur. While beyond the scope of this paper, we believe this issue could be addressed by refining the fitting algorithm or by using another unbiased fit to interpolate and smooth the experimental data. Here, our primary objective is to achieve a largely bias-free extrapolation to $t = 0$ and smooth data for short times, enabling the application of the inertia correction described in the following section. Without this step, applying the inertia correction using Eq. (8) would be impossible without discarding the high-frequency data of interest or manually optimizing the normalization and smoothing the short-time data as done in earlier work [7, 54]. With our approach, however, the inertia correction is stable and reproducible in all cases we examined. Fig. 2 shows a merged dataset along with the CONTIN fit to the data for $t \leq 5 \times 10^{-4}$ s. We replace the experimental data with the fit values over the range covered and normalize the data using the value of the fitted curve at $t \rightarrow 0$. This modified dataset is then used for further analysis. In the inset of Fig. 2, we show three repetitions of the same experiment shown in the main panel to demonstrate its stability and reproducibility.

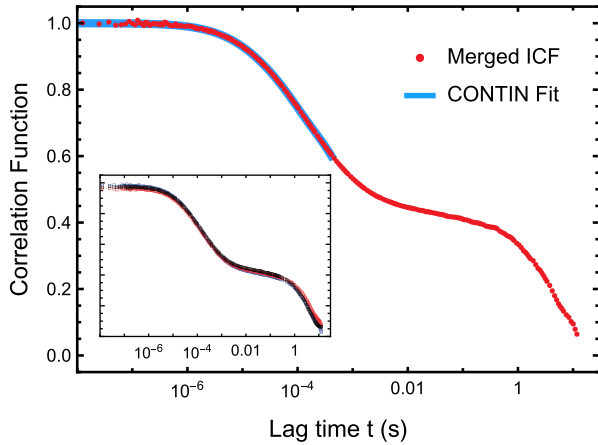


FIG. 2. CONTIN fit. Red circles: Merged correlation function $g_2(t) - 1$ as shown in Figure 1(c). Blue line: CONTIN-regularized fit to the correlation function for times $t \leq 5 \times 10^{-4}$ s. Both curves are normalized using the CONTIN fit extrapolated to $t = 0$. Inset: Merged $g_2(t) - 1$ from three repetitions of the experiment at $T = 20^\circ\text{C}$.

3. Microrheology

We determine the samples mean free path to $\ell^* \simeq 325\mu\text{m}$ using the commercial DWS RheoLab instrument (LS Instruments, Switzerland) along with the known values of $L = 2\text{mm}$ and $k = \frac{2\pi n}{\lambda} = 13.2\mu\text{m}^{-1}$, for $n_{\text{water}} = 1.33$, see also Figure S4. From this, we extract the particle mean squared displacement $\langle \Delta r^2(t) \rangle$ using Eq. (4) and the data is shown in Fig. 3. To smooth the data for times where the CONTIN fit was not applied, we use a sixth-order polynomial fit, shown in Fig. 3, as is commonly done [25], and replace the data for $t \geq 5 \times 10^{-4}$ s with the fitted values. We note once again that using a polynomial fit at very short times is not advisable, as the mean squared displacement exhibits a very complex time dependence due to the effects of inertia. With knowledge of the bead radius ($a = 210\text{nm}$), we determine the apparent complex modulus $Z^*(\omega)$ using Eq. (7) and the result is shown in Fig. 4 (a). Finally we apply Eq. (8) to account for the fluid and bead inertia, obtaining the true moduli of the sample, shown in Fig. 4 (b). The following values are used: $\rho_b = 1050\text{kg/m}^3$ (polystyrene bead mass density) and $\rho \simeq 1000\text{kg/m}^3$ (medium density). The water viscosity is $\eta_s = 1.02\text{mPas}$ at $T = 20^\circ\text{C}$.

In the high-frequency limit, we truncated the data at $\omega \simeq 5 \times 10^6\text{rad/s}$, above which the ICF decays by less 0.5% from 1 to 0.995. Using larger L/ℓ^* leads to a faster decay and may provide access to even higher frequencies. However, as seen in Fig. 4 (b), the complex modulus gradually approaches the modulus of the solvent $G''(\omega) = \eta_s \omega$. Thus, the upper bound for a stable DWS high-frequency analysis remains to be determined and is likely system dependent. Using the improved DWS implementation, we are already pushing the boundaries of the technique. Still, both the blending and merging procedure as well as the inertia correction are stable, and the process

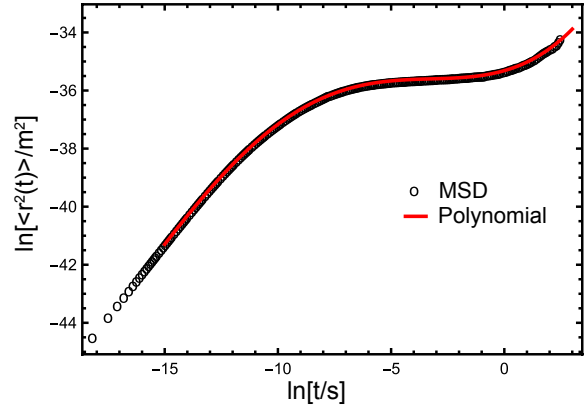


FIG. 3. Open red circles: Natural Logarithm of the mean squared particle displacement (MSD) calculated from the intensity correlation function via Eq. (4). Solid line: Polynomial fit of order six to the data displayed for times $t \geq 3 \times 10^{-7}$ s.

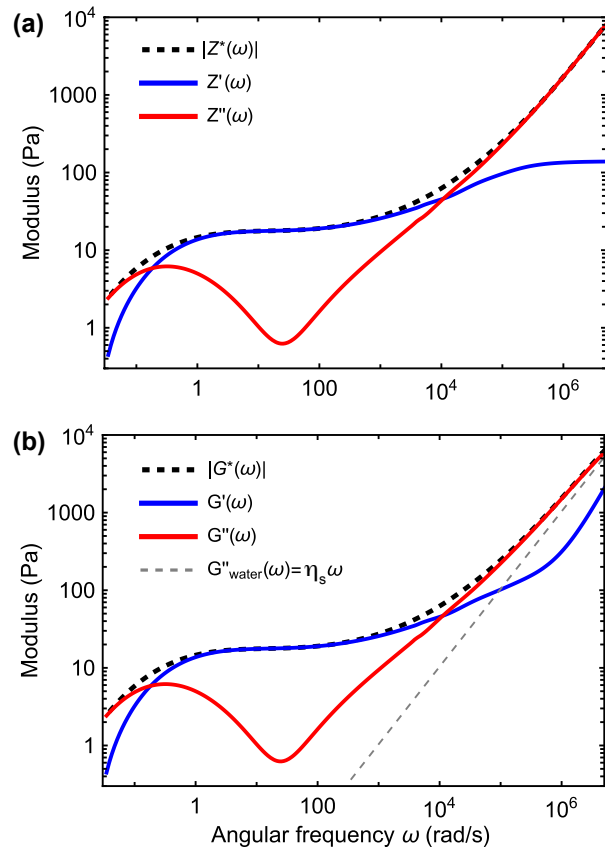


FIG. 4. (a) Apparent complex moduli of the micellar solution $Z^*(\omega)$ at $T = 20^\circ\text{C}$, as well as the real and the imaginary part $Z'(\omega), Z''(\omega)$, obtained using the Generalized Stokes-Einstein Relation (GSE), Eq. (7), and Mason's routine to convert the mean squared displacement [50]. (b) Corrected complex modulus of the sample after accounting for bead and fluid inertia, which primarily affects data at frequencies $\omega \geq 10^5\text{rad/s}$. The solvent loss modulus $G''(\omega) = \eta_s \omega$ is shown as a dashed line. The data is truncated at $\omega = 5 \times 10^6\text{rad/s}$.

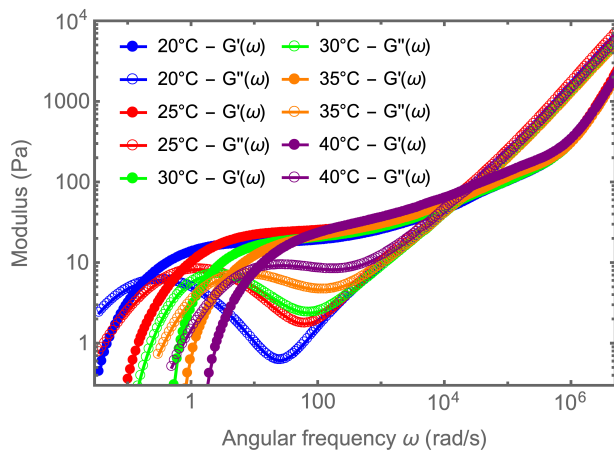


FIG. 5. Microrheology of the micellar solution at different temperatures, ranging from $T = 20^\circ\text{C}$ to $T = 40^\circ\text{C}$, illustrating the improved two-cell echo diffusing wave spectroscopy and tracer bead microrheology.

is highly reproducible.

For a practical test, we apply our method to study the viscoelastic moduli by performing a temperature ramp. Analogous experiments were reported earlier by Oelschlaeger et al., and our data compares quantitatively to this literature data [59]. While the previously published data was truncated at $\omega \simeq 10^5$ rad/s, here we extend the frequency range reproducibly for all temperatures up to $\omega \simeq 5 \times 10^6$ rad/s.

IV. CONCLUSIONS

In the present work, we presented a new implementation of two-cell echo diffusing wave spectroscopy (DWS) aimed at significantly improving the data quality and stability and thus extending the reach of DWS and DWS-based tracer bead microrheology. We replaced the standard calibration method for two-cell DWS, introduced by Romer et al. in 2000 [36], later used by many others and implemented in commercial DWS equipment [13, 29, 41], with a calibration-free approach. The new method generically corrects small fluctuations in the terminal decay time arising from imperfect temporal averaging, allowing for a seamless transition between two-cell DWS and

echo DWS. This smooth transition, in turn, facilitates a stable conversion of the bead mean square displacement to the complex viscoelastic modulus via the generalized Stokes-Einstein relation (GSER). Combined with the unbiased normalization of the correlation function using the CONTIN fit and the elimination of shot noise, the quality of DWS data is substantially improved. This enhancement enables the routine application of published formulas for correcting the effects of fluid and tracer bead inertia. As a result, the method provides unprecedented access to the high-frequency regime [7]. This capability will be beneficial for addressing questions related to the short-time dynamics of polymeric and other soft matter systems. Furthermore, this approach brings DWS closer to advanced techniques, such as neutron spin echo spectroscopy, connecting the high frequency viscoelastic relaxations to sub-microsecond scale dynamics in systems like microgels [63] or protein hydrogels [64].

ACKNOWLEDGMENTS

We thank Andrea Vaccaro (LS Instruments, Switzerland) for valuable discussions and assistance with the CONTIN fit algorithm. This work was financially supported by the Swiss National Science Foundation through project grant no. 10000141.

AUTHOR CONTRIBUTIONS

F.S. designed the study and wrote the Mathematica code. M.H. and C.Z. conducted the experiments. F.S. performed the data analysis with contributions from C.Z. and M.H. F.S. drafted the manuscript.

DATA AVAILABILITY STATEMENT

All experimental data and model output discussed in the manuscript will be uploaded to the repository Zenodo (xxxxxxx). All additional data sets generated during and/or analyzed during the current study are available from the corresponding author upon reasonable request.

-
- [1] D. Weitz, J. Zhu, D. Durian, H. Gang, and D. Pine, Diffusing-wave spectroscopy: The technique and some applications, *Physica Scripta* **1993**, 610 (1993).
 - [2] D. J. Pine, D. A. Weitz, J. Zhu, and E. Herbolzheimer, Diffusing-wave spectroscopy: dynamic light scattering in the multiple scattering limit, *Journal de Physique* **51**, 2101 (1990).
 - [3] D. J. Pine and D. A. Weitz, Diffusing-wave spectroscopy, in *Dynamic Light Scattering: The Method and Some Applications*, edited by W. Brown (Oxford University Press, Oxford, 1993) pp. 652–720.
 - [4] G. Maret, Diffusing-wave spectroscopy, *Current Opinion in Colloid & Interface Science* **2**, 251 (1997).
 - [5] J. Harden and V. Viasnoff, Recent advances in dws-based micro-rheology, *Current Opinion in Colloid & Interface Science* **6**, 438 (2001).
 - [6] B. R. Dasgupta, S.-Y. Tee, J. C. Crocker, B. Frisken, and D. Weitz, Microrheology of polyethylene oxide using diffusing wave spectroscopy and single scattering, *Physical Review E* **65**, 051505 (2002).
 - [7] N. Willenbacher, C. Oelschlaeger, M. Schopferer, P. Fischer, F. Cardinaux, and F. Scheffold, Broad bandwidth optical and

- mechanical rheometry of wormlike micelle solutions, *Physical Review Letters* **99**, 068302 (2007).
- [8] J. Galvan-Miyoshi, J. Delgado, and R. Castillo, Diffusing wave spectroscopy in maxwellian fluids, *The European Physical Journal E* **26**, 369 (2008).
- [9] Z. Fahimi, F. J. Aangenenendt, P. Voudouris, J. Mattsson, and H. M. Wyss, Diffusing-wave spectroscopy in a standard dynamic light scattering setup, *Physical Review E* **96**, 062611 (2017).
- [10] Z. Xing, A. Caciagli, T. Cao, I. Stoev, M. Zupkauskas, T. O'Neill, T. Wenzel, R. Lamboll, D. Liu, and E. Eiser, Microrheology of dna hydrogels, *Proceedings of the National Academy of Sciences* **115**, 8137 (2018).
- [11] V. Lorusso, D. Orsi, F. Salerno, L. Liggieri, F. Ravera, R. McMillin, J. Ferri, and L. Cristofolini, Recent developments in emulsion characterization: Diffusing wave spectroscopy beyond average values, *Advances in Colloid and Interface Science* **288**, 102341 (2021).
- [12] K. A. Dennis, Q. Li, N. Sbalbi, S. C. Brown, and E. M. Furst, Diffusing wave spectroscopy measurements of colloidal suspension dynamics, *Langmuir* **40**, 6129 (2024).
- [13] F. Scheffold, Light scattering and propagation in turbid media, in *Neutrons, X-rays, and light: scattering methods applied to soft condensed matter*, edited by P. Lindner and J. Oberdisse (Elsevier, 2024) pp. 581–610.
- [14] G. Maret and P. Wolf, Multiple light scattering from disordered media. the effect of brownian motion of scatterers, *Zeitschrift für Physik B Condensed Matter* **65**, 409 (1987).
- [15] D. J. Pine, D. A. Weitz, P. M. Chaikin, and E. Herbolzheimer, Diffusing wave spectroscopy, *Phys. Rev. Lett.* **60**, 1134 (1988).
- [16] B. J. Berne and R. Pecora, *Dynamic light scattering: with applications to chemistry, biology, and physics* (Courier Corporation, 2000).
- [17] F. Scheffold, S. Skipetrov, S. Romer, and P. Schurtenberger, Diffusing-wave spectroscopy of nonergodic media, *Physical Review E* **63**, 061404 (2001).
- [18] D. A. Boas, L. Campbell, and A. G. Yodh, Scattering and imaging with diffusing temporal field correlations, *Physical Review Letters* **75**, 1855 (1995).
- [19] D. A. Boas and A. G. Yodh, Spatially varying dynamical properties of turbid media probed with diffusing temporal light correlation, *JOSA A* **14**, 192 (1997).
- [20] X. Qiu, X. Wu, J. Xue, D. Pine, D. Weitz, and P. M. Chaikin, Hydrodynamic interactions in concentrated suspensions, *Physical Review Letters* **65**, 516 (1990).
- [21] L. Rojas-Ochoa, S. Romer, F. Scheffold, and P. Schurtenberger, Diffusing wave spectroscopy and small-angle neutron scattering from concentrated colloidal suspensions, *Physical Review E* **65**, 051403 (2002).
- [22] Q. Li, K. A. Dennis, Y.-F. Lee, and E. M. Furst, Two-point microrheology and diffusing wave spectroscopy, *Journal of Rheology* **67**, 1107 (2023).
- [23] H. S. Kim, N. Şenbil, C. Zhang, F. Scheffold, and T. G. Mason, Diffusing wave microrheology of highly scattering concentrated monodisperse emulsions, *Proceedings of the National Academy of Sciences* **116**, 7766 (2019).
- [24] Y. Xu and T. G. Mason, Jamming and depletion in extremely bidisperse mixtures of microscale emulsions and nanoemulsions, *Science Advances* **9**, eadh3715 (2023).
- [25] T. G. Mason and D. A. Weitz, Optical measurements of frequency-dependent linear viscoelastic moduli of complex fluids, *Physical Review Letters* **74**, 1250 (1995).
- [26] M. L. Gardel, M. T. Valentine, and D. A. Weitz, *Microrheology, in Microscale diagnostic techniques* (Springer, 2005) pp. 1–49.
- [27] T. A. Waigh, Microrheology of complex fluids, *Reports on progress in physics* **68**, 685 (2005).
- [28] E. M. Furst and T. M. Squires, *Microrheology* (Oxford University Press, 2017).
- [29] C. Zhang, M. Reufer, D. Gaudino, and F. Scheffold, Improved diffusing wave spectroscopy based on the automatized determination of the optical transport and absorption mean free path, *Korea-Australia Rheology Journal* **29**, 241 (2017).
- [30] I. D. Block and F. Scheffold, Modulated 3d cross-correlation light scattering: Improving turbid sample characterization, *Review of Scientific Instruments* **81** (2010).
- [31] D. A. Weitz, D. J. Pine, P. N. Pusey, and R. Tough, Nondiffusive brownian motion studied by diffusing-wave spectroscopy, *Physical Review Letters* **63**, 1747 (1989).
- [32] H. M. Wyss, S. Romer, F. Scheffold, P. Schurtenberger, and L. J. Gauckler, Diffusing-wave spectroscopy of concentrated alumina suspensions during gelation, *Journal of Colloid and Interface Science* **241**, 89 (2001).
- [33] F. Gittes and F. MacKintosh, Dynamic shear modulus of a semiflexible polymer network, *Physical Review E* **58**, R1241 (1998).
- [34] F. Gittes, B. Schnurr, P. Olmsted, F. C. MacKintosh, and C. F. Schmidt, Microscopic viscoelasticity: shear moduli of soft materials determined from thermal fluctuations, *Physical Review Letters* **79**, 3286 (1997).
- [35] A. J. Levine and T. Lubensky, Response function of a sphere in a viscoelastic two-fluid medium, *Physical Review E* **63**, 041510 (2001).
- [36] S. Romer, F. Scheffold, and P. Schurtenberger, Sol-gel transition of concentrated colloidal suspensions, *Physical Review Letters* **85**, 4980 (2000).
- [37] P. N. Pusey and W. Van Megen, Dynamic light scattering by non-ergodic media, *Physica A: Statistical Mechanics and its Applications* **157**, 705 (1989).
- [38] J.-Z. Xue, D. Pine, S. Milner, X.-L. Wu, and P. Chaikin, Non-ergodicity and light scattering from polymer gels, *Physical Review A* **46**, 6550 (1992).
- [39] A. Knaebel, M. Bellour, J.-P. Munch, V. Viasnoff, F. Lequeux, and J. Harden, Aging behavior of laponite clay particle suspensions, *Europhysics Letters* **52**, 73 (2000).
- [40] F. Cardinaux, L. Cipelletti, F. Scheffold, and P. Schurtenberger, Microrheology of giant-micelle solutions, *Europhysics Letters* **57**, 738 (2002).
- [41] V. Viasnoff, F. Lequeux, and D. Pine, Multispeckle diffusing-wave spectroscopy: A tool to study slow relaxation and time-dependent dynamics, *Review of Scientific Instruments* **73**, 2336 (2002).
- [42] P. Zakharov, F. Cardinaux, and F. Scheffold, Multispeckle diffusing-wave spectroscopy with a single-mode detection scheme, *Physical Review E—Statistical, Nonlinear, and Soft Matter Physics* **73**, 011413 (2006).
- [43] K. Pham, S. Egelhaaf, A. Moussaid, and P. Pusey, Ensemble-averaging in dynamic light scattering by an echo technique, *Review of Scientific Instruments* **75**, 2419 (2004).
- [44] S. Zhang, J. Peuser, C. Zhang, F. Cardinaux, P. Zakharov, S. E. Skipetrov, R. Cerbino, and F. Scheffold, Echo speckle imaging of dynamic processes in soft materials, *Optics Express* **30**, 30991 (2022).
- [45] K. Schätzel, Noise in photon correlation and photon structure functions, *Optica Acta: International Journal of Optics* **30**, 155 (1983).
- [46] J. Yoon, F. Cardinaux, C. Lapointe, C. Zhang, T. G. Mason, K. H. Ahn, and F. Scheffold, Brownian dynamics of colloidal microspheres with tunable elastic properties from soft to hard, *Colloids and Surfaces A: Physicochemical and Engineering As-*

- pects **546**, 360 (2018).
- [47] S. W. Provencher, A constrained regularization method for inverting data represented by linear algebraic or integral equations, *Computer Physics Communications* **27**, 213 (1982).
- [48] A. e. Scotti, W. Liu, J. Hyatt, E. Herman, H. Choi, J. Kim, L. Lyon, U. Gasser, and A. Fernandez-Nieves, The contin algorithm and its application to determine the size distribution of microgel suspensions, *The Journal of Chemical Physics* **142** (2015).
- [49] P.-A. Lemieux, M. Vera, and D. J. Durian, Diffusing-light spectroscopies beyond the diffusion limit: The role of ballistic transport and anisotropic scattering, *Physical Review E* **57**, 4498 (1998).
- [50] T. G. Mason, Estimating the viscoelastic moduli of complex fluids using the generalized stokes–einstein equation, *Rheologica acta* **39**, 371 (2000).
- [51] A. Einstein *et al.*, On the motion of small particles suspended in liquids at rest required by the molecular-kinetic theory of heat, *Annalen der Physik* **17**, 208 (1905).
- [52] E. J. Hinch, Application of the langevin equation to fluid suspensions, *Journal of Fluid Mechanics* **72**, 499 (1975).
- [53] R. Huang, I. Chavez, K. M. Taute, B. Lukić, S. Jeney, M. G. Raizen, and E.-L. Florin, Direct observation of the full transition from ballistic to diffusive brownian motion in a liquid, *Nature Physics* **7**, 576 (2011).
- [54] P. Domínguez-García, F. Cardinaux, E. Bertseva, L. Forró, F. Scheffold, and S. Jeney, Accounting for inertia effects to access the high-frequency microrheology of viscoelastic fluids, *Physical Review E* **90**, 060301 (2014).
- [55] T. Indei, J. D. Schieber, and A. Córdoba, Competing effects of particle and medium inertia on particle diffusion in viscoelastic materials, and their ramifications for passive microrheology, *Physical Review E—Statistical, Nonlinear, and Soft Matter Physics* **85**, 041504 (2012).
- [56] D. Mizuno, D. Head, F. MacKintosh, and C. Schmidt, Active and passive microrheology in equilibrium and nonequilibrium systems, *Macromolecules* **41**, 7194 (2008).
- [57] I. Wolfram Research, *Mathematica, Version 14.0*, Wolfram Research, Inc., Champaign, IL (2024).
- [58] P. Fischer and H. Rehage, Rheological master curves of viscoelastic surfactant solutions by varying the solvent viscosity and temperature, *Langmuir* **13**, 7012 (1997).
- [59] C. Oelschlaeger, M. Schopferer, F. Scheffold, and N. Willenbacher, Linear-to-branched micelles transition: A rheometry and diffusing wave spectroscopy (dws) study, *Langmuir* **25**, 716 (2009).
- [60] K. Schaetzel and R. Peters, Noise on multiple-tau photon correlation data, in *Photon Correlation Spectroscopy: Multicomponent Systems*, Vol. 1430 (SPIE, 1991) pp. 109–115.
- [61] M. Alexander and D. G. Dalgleish, Diffusing wave spectroscopy of aggregating and gelling systems, *Current Opinion in Colloid & Interface Science* **12**, 179 (2007).
- [62] X. Xue, X. Miao, J. Liu, Y. Ding, Y. Zhang, Y. Sun, W. Huang, Q. Jiang, B. Jiang, and S. Komarneni, Investigating the ph-dependence of gelation process in chitosan-glutaraldehyde hydrogels with diffusing wave spectroscopy, *Polymer* **316**, 127827 (2025).
- [63] Y. Hertle, M. Zeiser, P. Fouquet, M. Maccarini, and T. Hellweg, The internal network dynamics of poly (nipam) based copolymer micro-and macrogels: A comparative neutron spin-echo study, *Zeitschrift für Physikalische Chemie* **228**, 1053 (2014).
- [64] A. Rao, B. R. Carrick, H. Yao, and B. D. Olsen, Hindered segmental dynamics in associative protein hydrogels studied by neutron spin-echo spectroscopy, *Physical Review Materials* **7**, 075602 (2023).

Supplemental Material

SUPPLEMENTARY FIGURES

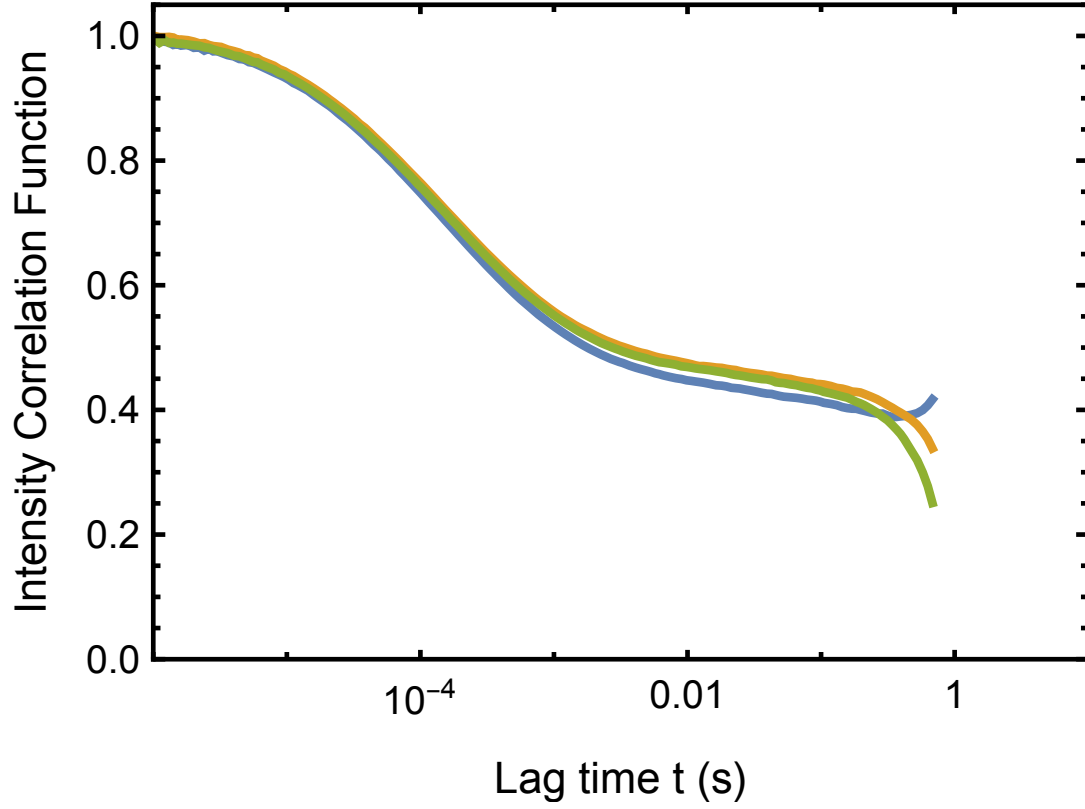


FIG. S1. Two-cell DWS using the conventional calibration with a solid reference sample (Teflon). The data corresponds to that shown in Figure 1 of the main text, taken at $T = 20^\circ\text{C}$. Here, we divided the recorded $g_2^{\text{TC}}(t) - 1$ by the ICF of the solid calibration sample, $g_2^{\text{2nd}}(t) - 1$, shown as a dashed line in Figure 1 (a). The resulting $(g_2(t) - 1)$ for three repetitions is shown and plotted up to $t = \tau_{\text{TC}}$. Merging the data with $(g_2^{\text{Echo}}(t) - 1)$ may lead to an unsteady curve with a kink in many cases, most prominently in the present example for the blue line.

Experiment No.	Amplitude A	Decay Time τ_{TC} [s]
1	0.850782	0.287184
2	0.763751	0.286332
3	0.752708	0.287966
4	0.794214	0.275153
5	0.755180	0.277028

TABLE S1. Summary of experimental results showing the fitted amplitude and decay time for each of the experiments shown in Fig. S3. The mean values are $\langle A \rangle = 0.7833 \pm 0.0368$ and $\langle \tau_{\text{TC}} \rangle = 0.2827 \pm 0.0055$.

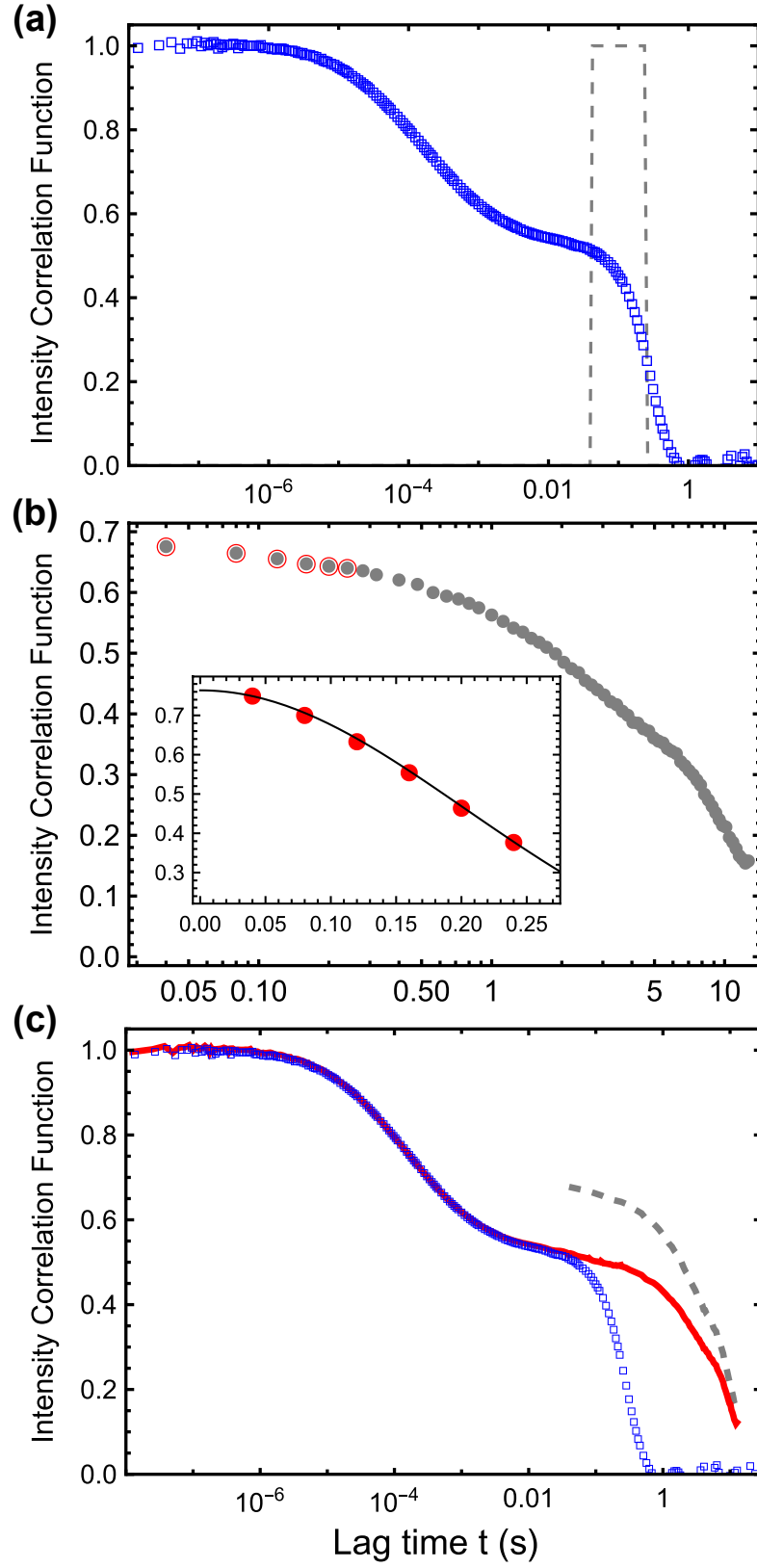


FIG. S2. Same experiment as in Figure 1, but with 2.5 times faster motion of the diffuser during the two-cell measurement, leading to $\tau_{TC} \simeq 0.28$ s. The value of $\ell^* \simeq 413 \mu\text{m}$ is slightly higher due to minor settling of the tracer beads. In the overlap region, indicated by the dashed lines in panel (a), where the two datasets are blended and merged, the TC-ICF now decays to about one-half, $e^{-(6\tau_{\text{Echo}}/0.28 \text{ s})^2} \simeq 1/2$. The fit with Eq. (2) remains excellent and stable, and the merged ICF is continuous and smooth, as shown in panels (b) and (c).

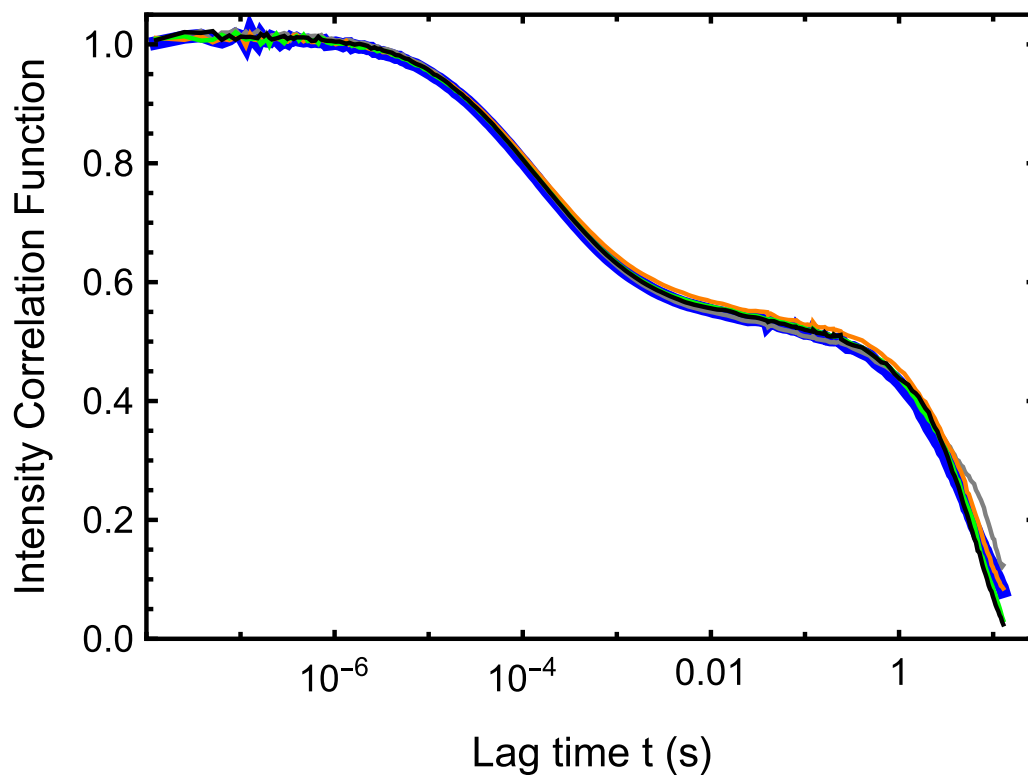


FIG. S3. Five repetitions of the experiment shown in Fig. S1. The measurement times are 300 seconds for the TC-DWS and 60 seconds for the Echo-DWS. The fitted parameters A and τ_{TC} are listed in Table S1.

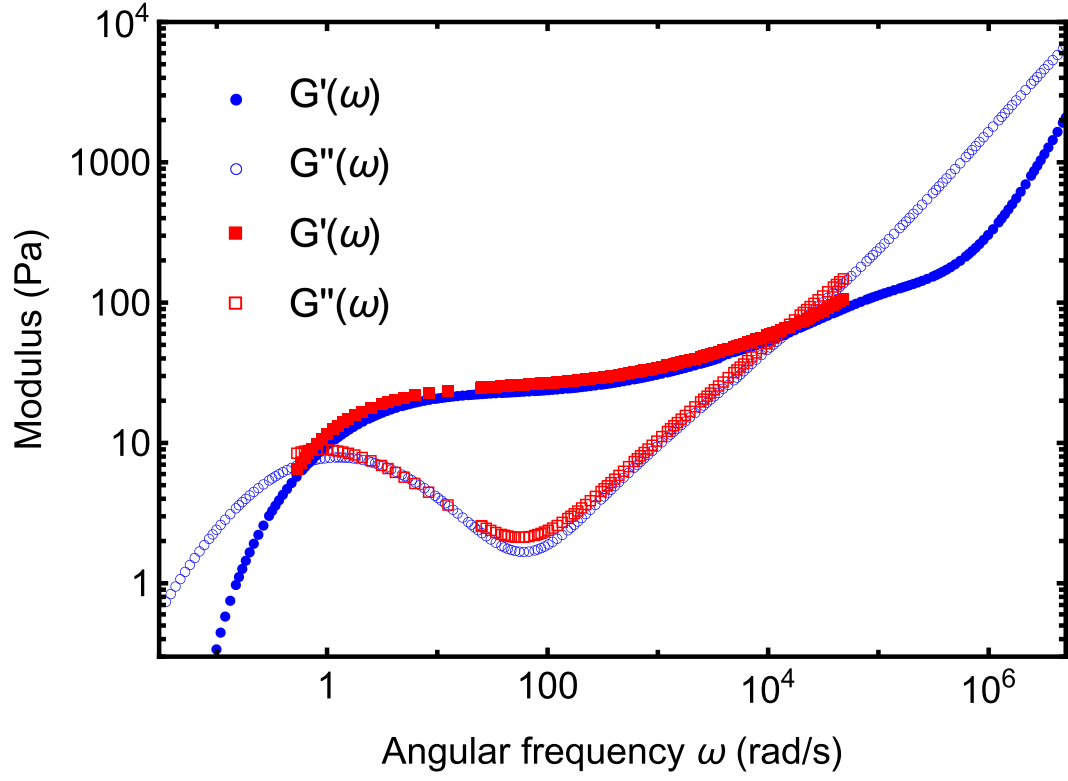


FIG. S4. Comparison of the $T = 25^\circ\text{C}$ data obtained using a commercial DWS instrument (red symbols), DWS RheoLab (LS Instruments, Switzerland), and the data obtained with our DWS microrheology implementation, as shown in Fig. 5 of the manuscript (blue symbols). The exact same sample contained in a $L = 2$ mm cuvette was analyzed. Storage modulus $G'(\omega)$ and loss modulus $G''(\omega)$ are shown as full and open symbols, respectively.